


## Rotational dynamics of O<sub>2</sub> in the electronic ground $X^3\Sigma_g^-$ state induced by an intense femtosecond laser field

Kotaro Sonoda,<sup>1</sup> Shinichi Fukahori <sup>1,2</sup> and Hirokazu Hasegawa <sup>1,2,\*</sup>

<sup>1</sup>*Department of Integrated Sciences, Graduate School of Arts and Sciences, The University of Tokyo, Komaba, Meguro-ku, Tokyo 153-8902, Japan*

<sup>2</sup>*Komaba Institute for Science, The University of Tokyo, Komaba, Meguro-ku, Tokyo 153-8902, Japan*

 (Received 13 January 2021; revised 5 March 2021; accepted 16 March 2021; published 26 March 2021)

We theoretically and numerically investigate rotational dynamics of O<sub>2</sub> in the electronic  $X^3\Sigma_g^-$  ground state induced by an intense femtosecond laser field. The rotational dynamics are calculated by two different models. One of the models includes triplet splittings explicitly in rotational energy levels originated from an electronic spin (a spin-dependent model), and the other omits the triplet splittings (a spin-independent model). We find that the final rotational population after the interaction with the laser field does not depend on the models. On the other hand, we find that the rotational dynamics evaluated by alignment degrees and angular distributions of molecular axes depend on the models. Although the rotational dynamics calculated by the spin-independent model is similar to that calculated by the spin-dependent model within 5 ps, the triplet splittings in the rotational energy levels affect the rotational dynamics after 5 ps. This is explained by the inverse of the energy difference between triplet splittings in the rotational levels. We show that the multiplet energy splittings in rotational energies should be included when the rotational dynamics in the multiplet electronic state are considered. We also investigate excitation processes on the basis of time evolutions of state populations and find that there are excitation pathways with double as well as single bifurcations depending on the initial state.

DOI: [10.1103/PhysRevA.103.033118](https://doi.org/10.1103/PhysRevA.103.033118)

### I. INTRODUCTION

The coherent rotational dynamics of molecules induced by an intense laser field with a shorter temporal duration than a rotational period causes transient and periodic alignment of molecular axes, commonly known as nonadiabatic molecular alignment, transient molecular alignment, and impulsive alignment, which has been widely investigated [1–3] since early theoretical studies [4–6] and experimental observations [7,8]. The rotational dynamics are observed by various pump-probe techniques based on the angular distribution of the fragment ions [8], the yield of the high-order harmonics [9], the optical birefringence [7,10], and the balanced weak-field polarization technique [11]. The real-time movie of the molecular rotation has been recently reported [12,13]. Since the rotational dynamics and the transient molecular alignment depend on structures of rotational energy levels, various types of molecules such as linear molecules [8,10,11,14–26], symmetric top molecules [27–30], and asymmetric top molecules [31–36] have been thoroughly studied.

In addition to molecular structure, angular momenta such as electronic orbital, electronic spin, vibrational, and nuclear-spin angular momenta influence rotational energy-level structures. Therefore, many angular momenta play an essential role in rotational dynamics. However, angular momenta of almost all stable molecules in an electronic ground state are quenched. Most previous studies on the rotational dynamics were focused on closed-shell molecules in an

electronic ground  $^1\Sigma$  state such as N<sub>2</sub> [9,15], I<sub>2</sub> [8], CO<sub>2</sub> [15,26,37], and C<sub>2</sub>H<sub>2</sub> [38,39].

On the other hand, radical molecules with an unpaired electron(s) are expected to show peculiar rotational dynamics due to unquenched electronic angular momenta. For example, the rotational dynamics of the NO radical showed that the rotational period (the full revival period) is given by  $T_{\text{rot}} = \frac{1}{cB}$  instead of  $T_{\text{rot}} = \frac{1}{2cB}$ , which is the rotational period for closed-shell linear molecules, where  $c$  is the speed of the light in vacuum and  $B$  is the rotational constant [40], and that the selection rule,  $\Delta J = \pm 1, \pm 2$ , for the excitation induced by the intense laser field differs from that for closed-shell molecules, where  $J$  is the total angular momentum quantum number. In addition to the rotational, electronic orbital, and spin angular momenta, nuclear-spin angular momenta contribute to the total angular momentum in a molecule. The rotational dynamics coupled with the nuclear spin has been observed in real-time measurement [41,42].

The rotational dynamics of the O<sub>2</sub> molecule, which has a resultant electronic spin angular momentum originated from two unpaired  $\pi$  electrons in the electronic ground  $X^3\Sigma_g^-$  state, was also investigated [11,15,16,37,43,44]. In most of the past studies, the O<sub>2</sub> molecule was approximated as a spinless molecule, and the effect of the electronic spin on the rotational dynamics has not been taken into account. A few studies on the rotational dynamics of O<sub>2</sub> including explicitly the electronic spin were reported [45–47].

In this paper, the rotational dynamics of the O<sub>2</sub> molecule calculated by a spin-dependent model as well as a spin-independent model are compared. In the spin-independent model, an effect of the electronic spin is ignored. The

\*chs36@mail.ecc.u-tokyo.ac.jp

rotational eigenenergy and eigenfunction are described by  $E_N = BN(N + 1)$  and spherical harmonics, respectively. On the other hand, in the spin-dependent model, the triplet character of the rotational energy due to the electronic spin angular momentum is explicitly considered, and the rotational eigenfunction is expressed by Hund's case (b) wave functions. The effect of the electronic spin on the rotational dynamics is discussed.

## II. THEORY

The Hamiltonian  $\hat{H}$ , including the free rotation  $\hat{H}_{\text{rot}}$ , the spin-spin interaction  $\hat{H}_{\text{SS}}$ , and the spin-rotation interaction  $\hat{H}_{\text{SR}}$ , of  $\text{O}_2$  in the vibrational ground state in the electronic ground  $X^3\Sigma_g^-$  state is expressed as follows [48,49]:

$$\hat{H} = \hat{H}_{\text{rot}} + \hat{H}_{\text{SS}} + \hat{H}_{\text{SR}}, \quad (1)$$

$$\hat{H}_{\text{rot}} = B\hat{N}^2, \quad (2)$$

$$\hat{H}_{\text{SS}} = \frac{2}{3}\lambda(3\hat{S}_z^2 - S^2), \quad (3)$$

$$\hat{H}_{\text{SR}} = \gamma\hat{N} \cdot \hat{S}, \quad (4)$$

where  $\hat{N}$ ,  $\hat{S}$ , and  $\hat{S}_z$  are the angular momenta of molecular rotation, electronic spin, and the projection of  $\hat{S}$  onto the molecular axis (defined as the  $z$  axis), respectively, and  $B$ ,  $\lambda$ , and  $\gamma$  are rotational, electronic spin-spin coupling, and spin-rotation coupling constants, respectively.

In this paper, the rotational dynamics of  $\text{O}_2$  induced by an intense femtosecond laser field with a linear polarization are investigated by two models. One is a spin-independent model, in which the triplet splitting in rotational energy levels is not considered. Therefore, the interaction terms including the electronic spin,  $\hat{H}_{\text{SS}}$  and  $\hat{H}_{\text{SR}}$ , are neglected. In this model, an eigenstate is described by the direct product between the rotational states and electronic spin states,  $|N, M_N\rangle|S, M_S\rangle$ , where  $N(S)$  and  $M_N(M_S)$  represent the quantum numbers of the rotational (electronic spin) angular momentum and its projection onto a space-fixed  $Z$  axis parallel to the laser polarization direction, respectively. The rotational quantum number,  $N = 1, 3, 5, \dots$ , is limited to be odd numbers because of the nuclear-spin statistics originated from a  $^{16}\text{O}$

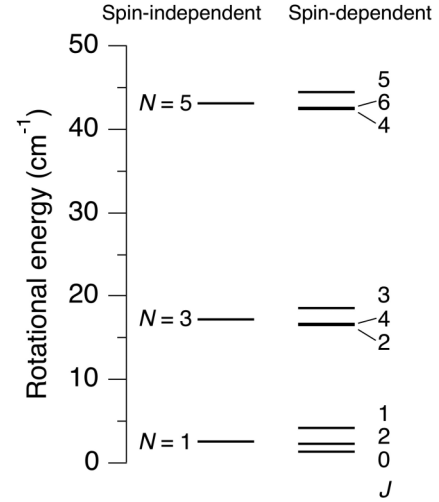


FIG. 1. The rotational energy diagram of  $\text{O}_2$  in the electronic ground  $X^3\Sigma_g^-$  state.

nucleus. The resultant electronic spin quantum number is fixed to be  $S = 1$  in the electronic ground  $X^3\Sigma_g^-$  state. The angular representation of the rotational state,  $|N, M_N\rangle$ , corresponds to the spherical harmonics,  $Y_{N, M_N}(\theta, \phi)$ , where  $\theta$  and  $\phi$  are the polar and azimuthal angles of a molecular axis with regard to the  $Z$  axis. The rotational energy is expressed by  $E = BN(N + 1)$  and depends only on  $N$  regardless of the electronic spin. This model disregarding the electronic spin has been widely adopted to analyze the molecular alignment of  $\text{O}_2$  [15,16].

In the other model explicitly including the effect of the electronic spin, hereafter called a spin-dependent model, the rotational state is described by the Hund's case (b) wave function,  $|(NS)JM_J\rangle$ , where  $J$  is the quantum number of the total angular momentum,  $\hat{J} = \hat{N} + \hat{S}$ , and  $M_J$  is the quantum number of the projection of the total angular momentum onto the  $Z$  axis. According to the addition rule of two angular momenta, the allowed  $J$  values are  $N - 1, N$ , and  $N + 1$  for a given  $N$ . The diagonal matrix elements of the Hamiltonian, Eq. (1), evaluated using the Hund's case (b) basis set are obtained as the following expressions [48–50]:

$$\langle (NS)JM_J | \hat{H} | (NS)JM_J \rangle = BN(N + 1) - \frac{2}{3}\lambda \frac{N + 1}{2N - 1} - \gamma(N + 1) \quad \text{for } J = N - 1, \quad (5)$$

$$\langle (NS)JM_J | \hat{H} | (NS)JM_J \rangle = BN(N + 1) + \frac{2}{3}\lambda - \gamma \quad \text{for } J = N, \quad (6)$$

$$\langle (NS)JM_J | \hat{H} | (NS)JM_J \rangle = BN(N + 1) - \frac{2}{3}\lambda \frac{N}{2N + 3} + \gamma N \quad \text{for } J = N + 1. \quad (7)$$

The small off-diagonal matrix elements are ignored in our model although the spin-spin interaction term,  $\hat{H}_{\text{SS}}$ , has the off-diagonal matrix elements with  $\Delta N = \pm 2$ . Therefore, the Hund's case (b) basis,  $|(NS)JM_J\rangle$ , is the eigenstate for the Hamiltonian, Eq. (1). By including  $\hat{H}_{\text{SS}}$  and  $\hat{H}_{\text{SR}}$ , there are three states with different energies for a given rotational quantum number,  $N$ , i.e., triplet states.

Figure 1 shows the rotational energy diagram of  $\text{O}_2$  in the electronic ground  $X^3\Sigma_g^-$  state. Each rotational state of  $N$  is triply degenerated for the spin-independent model due to the uncoupled spin states,  $|S = 1, M_S = -1, 0, 1\rangle$ . Each rotational state of  $N$  splits into three states for the spin-dependent model due to the spin interactions,  $\hat{H}_{\text{SS}}$  and  $\hat{H}_{\text{SR}}$ .

The interaction of the molecular anisotropic polarizability with a linearly polarized intense laser field is generally written as

$$V(t) = -\frac{1}{2}\alpha_{ZZ}E_Z^2(t), \quad (8)$$

where  $\alpha_{ZZ}$  is a ZZ component of a molecular polarizability tensor in a space-fixed coordinate system and  $E_Z(t)$  is an electric field of the intense laser field with the polarization direction parallel to the Z axis [1–3]. The electric field is assumed to be  $E_Z(t) = E_0(t) \cos(\omega t + \delta)$  where  $E_0(t)$  is an envelope function, and  $\omega$  and  $\delta$  are an angular frequency and an initial phase of the laser field, respectively. The envelope

function of the laser field is assumed to be

$$E_0(t) = \exp\left\{-2 \ln 2 \left(\frac{t}{\Delta t}\right)^2\right\}, \quad (9)$$

where  $\Delta t$  is the pulse duration. Since the fast carrier wave of the electric field does not affect the molecular dynamics, the interaction potential averaged over one temporal cycle can be expressed as

$$\bar{V}(t) = -\frac{1}{4}\alpha_{ZZ}E_0^2(t). \quad (10)$$

This assumption is suitable for off-resonance conditions.

In the spin-independent model ignoring  $\hat{H}_{SS}$  and  $\hat{H}_{SR}$  in Eq. (1), the matrix elements of  $\bar{V}(t)$  can be expressed by

$$\langle S, M_S | \langle N, M_N | \bar{V}(t) | N, M_N \rangle | S, M_S \rangle = -\frac{1}{4}E_0^2(t) \left\{ \frac{1}{3} \frac{N(N+1) - 3M_N^2}{(2N+3)(2N-1)} \Delta\alpha + \bar{\alpha} \right\}, \quad (11)$$

$$\langle S, M_S | \langle N+2, M_N | \bar{V}(t) | N, M_N \rangle | S, M_S \rangle = -\frac{(-1)^{M_N}}{4}E_0^2(t) \Delta\alpha \frac{\sqrt{\{(N+2)^2 - M_N^2\}\{(N+1)^2 - M_N^2\}}}{(2N+5)(2N+3)}, \quad (12)$$

where  $\Delta\alpha = \alpha_{\parallel} - \alpha_{\perp}$  is an anisotropic polarizability;  $\alpha_{\parallel}$  and  $\alpha_{\perp}$  are the components of the polarizability parallel and perpendicular to the molecular axis, respectively; and  $\bar{\alpha} = \frac{1}{3}(\alpha_{\parallel} + 2\alpha_{\perp})$  is the averaged polarizability [2,3,51]. On the basis of these matrix elements, it is recognized that the intense laser field induces the transitions between rotational states  $N$  and  $N \pm 2$ . The  $M_N$  is preserved due to the axial symmetry of the interaction. The  $S$  and  $M_S$  are also conserved because of no interaction between the electronic spin and the intense laser field.

In the spin-dependent model, the interaction matrix element can be written as

$$\begin{aligned} & \langle (N_1 S) J_1 M_{J_1} | \bar{V}(t) | (N_2 S) J_2 M_{J_2} \rangle \\ &= -\frac{1}{4}E_0^2(t) \left[ (-1)^{J_1+J_2-M_{J_1}+1} \frac{2}{3} \sqrt{(2J_1+1)(2J_2+1)(2N_1+1)(2N_2+1)} \right. \\ & \quad \left. \times \begin{pmatrix} J_1 & 2 & J_2 \\ -M_{J_1} & 0 & M_{J_2} \end{pmatrix} \begin{pmatrix} N_1 & 2 & N_2 \\ 0 & 0 & 0 \end{pmatrix} \begin{Bmatrix} N_1 & J_1 & 1 \\ J_2 & N_2 & 2 \end{Bmatrix} \Delta\alpha + \bar{\alpha} \delta_{N_1, N_2} \delta_{J_1, J_2} \delta_{M_{J_1}, M_{J_2}} \right], \quad (13) \end{aligned}$$

where the symbols of  $\begin{pmatrix} \dots \end{pmatrix}$  and  $\begin{Bmatrix} \dots \end{Bmatrix}$  represent Wigner's 3- $j$  and 6- $j$  symbols, respectively [3,48]. The selection rules,  $\Delta N = 0, \pm 2$ ,  $\Delta M_J = 0$ , and  $\Delta J = 0, \pm 1, \pm 2$  ( $\Delta J = 0, \pm 2$  when  $M_{J_1} = M_{J_2} = 0$ ), are obtained from the 3- $j$  and 6- $j$  symbols. The spin quantum number,  $S = 1$ , is also conserved.

The interaction with the intense laser field changes the initial rotational states  $|N_0, M_{N_0}\rangle |S_0, M_{S_0}\rangle$  or  $|(N_0 S_0) J_0 M_{J_0}\rangle$  into the following wave packets for the spin-independent or -dependent models, respectively:

$$|\Psi_{\text{ind}}(t)\rangle = \sum_N c_N^{N_0, M_{N_0}, M_{S_0}}(t) e^{-i\frac{E_N}{\hbar}t} |N, M_{N_0}\rangle |S, M_{S_0}\rangle, \quad (14)$$

$$|\Psi_{\text{dep}}(t)\rangle = \sum_N \sum_J c_{NJ}^{N_0, J_0, M_{J_0}}(t) e^{-i\frac{E_{NJ}}{\hbar}t} |(NS) J M_{J_0}\rangle, \quad (15)$$

where  $c_N^{N_0, M_{N_0}, M_{S_0}}(t)$  and  $c_{NJ}^{N_0, J_0, M_{J_0}}(t)$  are the probability amplitudes for respective models,  $E_N$  is the rotational energy of the state  $|N, M_N\rangle |S, M_S\rangle$  for the spin-independent model, and  $E_{NJ}$  is the rotational energy of the state  $|(NS) J M_J\rangle$  for the spin-dependent model. The probability amplitudes are calculated by numerically solving the time-dependent Schrödinger equations (TDSEs):

$$i\hbar \frac{d}{dt} c_N^{N_0, M_{N_0}, M_{S_0}}(t) = \sum_{N'} c_{N'}^{N_0, M_{N_0}, M_{S_0}}(t) e^{-i\frac{(E_{N'} - E_N)}{\hbar}t} \langle N, M_{N_0} | \bar{V}(t) | N', M_{N_0} \rangle, \quad (16)$$

$$i\hbar \frac{d}{dt} c_{NJ}^{N_0, J_0, M_{J_0}}(t) = \sum_{N'} \sum_{J'} c_{N'J'}^{N_0, J_0, M_{J_0}}(t) e^{-i\frac{(E_{N'J'} - E_{NJ})}{\hbar}t} \langle (NS) J M_{J_0} | \bar{V}(t) | (N'S) J' M_{J_0} \rangle. \quad (17)$$

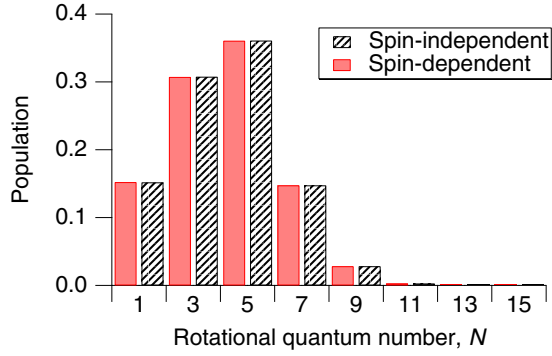


FIG. 2. The final rotational populations calculated by the spin-independent and dependent models. The intensity and pulse width of the intense laser field are 30 TW/cm<sup>2</sup> and 100 fs, respectively. The initial states are set to be an ensemble of three states,  $|N = 1, M_N = -1, 0, 1\rangle$ , with an equivalent statistical weight for the spin-independent model and nine states,  $|N = 1, J = 0, M_J = 0\rangle$ ,  $|N = 1, J = 1, M_J = -1, 0, 1\rangle$ ,  $|N = 1, J = 2, M_J = -2, -1, 0, 1, 2\rangle$ , with an equivalent statistical weight for the spin-dependent model.

### III. RESULTS AND DISCUSSION

Figure 2 shows the final rotational populations calculated by the spin-independent and -dependent models. The eigenfunctions up to  $N = 31$  are included in the calculation, and the laser intensity and the pulse duration are 30 TW/cm<sup>2</sup> and 100 fs, respectively. The rotational energy for the spin-dependent model,  $E_{NJ}$ , is calculated from rotational energy formulas [52] and molecular parameters [53]. The averaged values of  $E_{NJ=N-1}$ ,  $E_{NJ=N}$ , and  $E_{NJ=N+1}$  are used as the rotational energy for the spin-independent model,  $E_N$ . The rotational energy levels up to  $N = 5$  for each model are shown in Fig. 1. The initial states are set to be an ensemble of three states,  $|N = 1, M_N = -1, 0, 1\rangle$  for the spin-independent model. On the other hand, the initial states are set to be an ensemble of nine states,  $|N = 1, J = 0, M_J = 0\rangle$ ,  $|N = 1, J = 1, M_J = -1, 0, 1\rangle$ , and  $|N = 1, J = 2, M_J = -2, -1, 0, 1, 2\rangle$  for the spin-dependent model. The statistical weights of these initial states are assumed to be equal. These initial conditions correspond to the low-temperature limit because the initial states are degenerate for the spin-independent model and are almost degenerate for the spin-dependent model, in which the energy difference between the highest energy of 4.21 cm<sup>-1</sup> for the  $N = 1, J = 1$  state and the lowest energy of 1.31 cm<sup>-1</sup> for the  $N = 1, J = 0$  state is small.

The rotational state up to  $N = 9$  is excited by the intense laser field as shown in Fig. 2. The rotational state of  $N = 9$  is created by stepwise rotational Raman excitation from the initial state of  $N = 1$  due to the selection rule,  $\Delta N = \pm 2$ . This stepwise rotational Raman excitation by an intense laser field was reported for linear molecules such as N<sub>2</sub> [51] and NO [54,55].

It should be noted that the final populations calculated by two different models exhibit almost the same distributions. This result implies that the final population can be obtained by a calculation without considering the electronic spin. The relationship between the spin-independent basis function,  $|N, M_N\rangle|S, M_S\rangle$ , and the spin-dependent basis func-

tion,  $|(NS)JM_J\rangle$ , is given through the Clebsch-Gordan coefficient,  $\langle N, M_N, S, M_S|J, M\rangle$ , as follows [48,49]:

$$|(NS)JM_J\rangle = \sum_{M_N} \sum_{M_S} \langle N, M_N, S, M_S|J, M_J\rangle |N, M_N\rangle |S, M_S\rangle. \quad (18)$$

The probability amplitudes of the wave packet,  $c_{NJ}^{N_0, J_0, M_{J_0}}(t)$  and  $c_N^{N_0, M_{N_0}, M_{S_0}}(t)$  for the spin-dependent and -independent models, respectively, should also have a similar relationship due to the linearity of the TDSE as follows:

$$c_{NJ}^{N_0, J_0, M_{J_0}}(t) = \sum_{M_{N_0}} \sum_{M_{S_0}} \langle J, M_{J_0}|N, M_{N_0}, S, M_{S_0}\rangle c_N^{N_0, M_{N_0}, M_{S_0}}(t). \quad (19)$$

Here, the small energy difference between  $E_N$  and  $E_{NJ}$  for all  $J$  is neglected. This assumption is appropriate because the energy differences among triplet states are about 2 cm<sup>-1</sup> up to  $N = 9$ , which is much smaller than the rotational energy. The populations of the rotational state  $N$  for the spin-dependent and -independent models,  $P_N^{\text{ind}}$  and  $P_N^{\text{dep}}$ , are, respectively, defined by

$$P_N^{\text{ind}} = \sum_{M_{N_0}} \sum_{M_{S_0}} |c_N^{N_0, M_{N_0}, M_{S_0}}|^2, \quad (20)$$

$$P_N^{\text{dep}} = \sum_{J=N-1}^{N+1} \sum_{M_{J_0}} |c_{NJ}^{N_0, J_0, M_{J_0}}|^2. \quad (21)$$

The equation,  $P_N^{\text{ind}} = P_N^{\text{dep}}$ , can be obtained by using Eq. (19). Our result shows that the population calculated by the spin-independent model, i.e., using the spherical harmonics as the basis function, reproduces the population calculated by the spin-dependent model, i.e., using Hund's case (b) as the basis function.

In order to investigate rotational dynamics, the time evolution of the expectation value of  $\cos^2 \theta$ ,  $\langle \cos^2 \theta \rangle(t) = \langle \Psi_{\text{ind/dep}}(t) | \cos^2 \theta | \Psi_{\text{ind/dep}}(t) \rangle$ , is calculated by both models, where  $\theta$  represents the angle between the laser polarization direction and the molecular axis of O<sub>2</sub>. By considering the

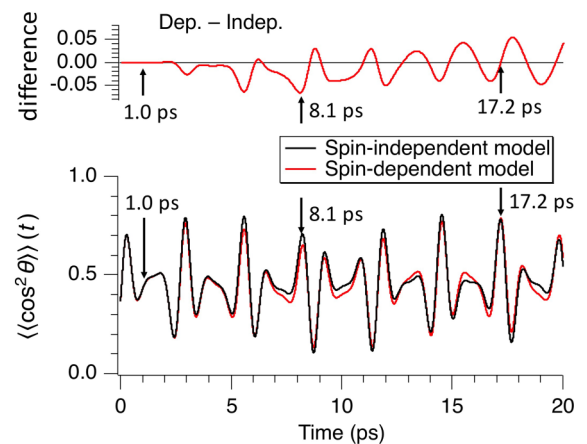


FIG. 3. The time evolution of  $\langle \cos^2 \theta \rangle(t)$  for spin-independent and -dependent models.

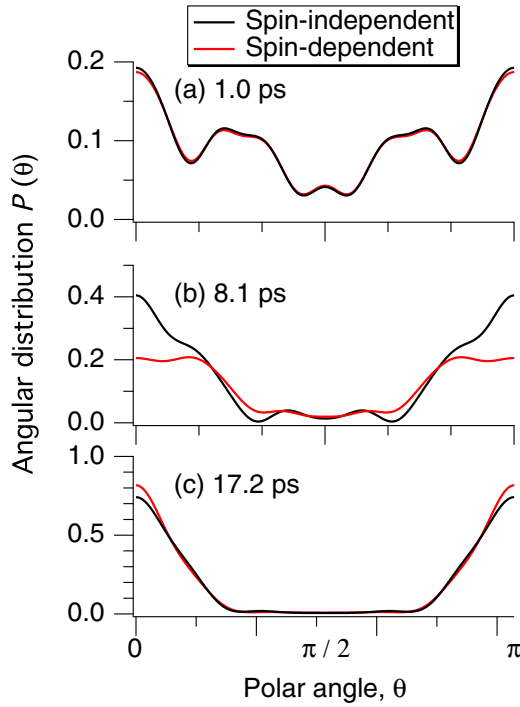


FIG. 4. The angular distribution of the O<sub>2</sub> molecular axis for the spin-dependent and -independent models at (a) 1.0 ps, (b) 8.1 ps, and (c) 17.2 ps after the interaction.

initial-state distribution as mentioned above, the averaged expectation values of  $\cos^2\theta$ ,  $\langle\langle\cos^2\theta\rangle\rangle(t)$ , are obtained as shown in the lower panel of Fig. 3. The periodic structure of  $\langle\langle\cos^2\theta\rangle\rangle(t)$  is clearly identified with the period of 11.6 ps for each model. The observed period agrees with the rotational period,  $T_{\text{rot}} = \frac{1}{2cB} = 11.6$  ps, where  $B = 1.4377$  cm<sup>-1</sup> is the

rotational constant [53]. The periodic transient signals of O<sub>2</sub> were observed by high-order harmonics [15] and four-wave mixing [16].

In Fig. 3, the comparison between the spin-independent and -dependent models clarifies that the  $\langle\langle\cos^2\theta\rangle\rangle(t)$  calculated by both models agrees well until about 5 ps. On the other hand, we found that the difference of  $\langle\langle\cos^2\theta\rangle\rangle(t)$  between the respective models as shown in the upper panel of Fig. 3 oscillates and its maximum value reaches  $-0.07$  at 8.1 ps. The rotational dynamics depends on the rotational energy through the factor of  $e^{-i\frac{E}{\hbar}t}$  in the wave packet, Eqs. (14) and (15). The maximum-energy difference between  $E_N$  and  $E_{NJ}$  is  $1.3$  cm<sup>-1</sup> for  $N \geq 3$  states. The difference starting at around 5 ps is explained by the maximum-energy difference of  $1.3$  cm<sup>-1</sup> for each model because the energy difference of  $1.3$  cm<sup>-1</sup> corresponds to the time difference of 4.1 ps in rotational dynamics on the basis of the uncertainty principle. Since the  $\langle\langle\cos^2\theta\rangle\rangle(t)$  calculated by the spin-independent model cannot reproduce that calculated by the spin-dependent model at the time later than 5 ps, the molecular axis distribution is also expected to be different for both models.

Figure 4 shows the calculated molecular axis distributions,  $P(\theta) = 2\pi|\langle\theta, \phi|\Psi_{\text{ind/dep}}(t)\rangle|^2$ , at  $t = 1.0, 8.1,$  and  $17.2$  ps. The molecular axis distributions are calculated by using the angular representation of the basis functions,  $\langle\theta, \phi|N, M_N\rangle = Y_{N, M_N}(\theta, \phi)$ , for the spin-dependent model. On the other hand, the angular representation of the Hund's case (b) basis functions represented by Hund's case (a),

$$\begin{aligned} \langle\theta, \phi|(NS)JM_J\rangle &= \sum_{\Sigma=-1}^1 (-1)^{J-S+\Lambda} \sqrt{2N+1} \\ &\times \begin{pmatrix} J & S & N \\ \Omega - \Sigma & -\Sigma & -\Lambda \end{pmatrix} \langle\theta, \phi|J, \Omega, M_J\rangle |S, \Sigma\rangle, \end{aligned} \quad (22)$$

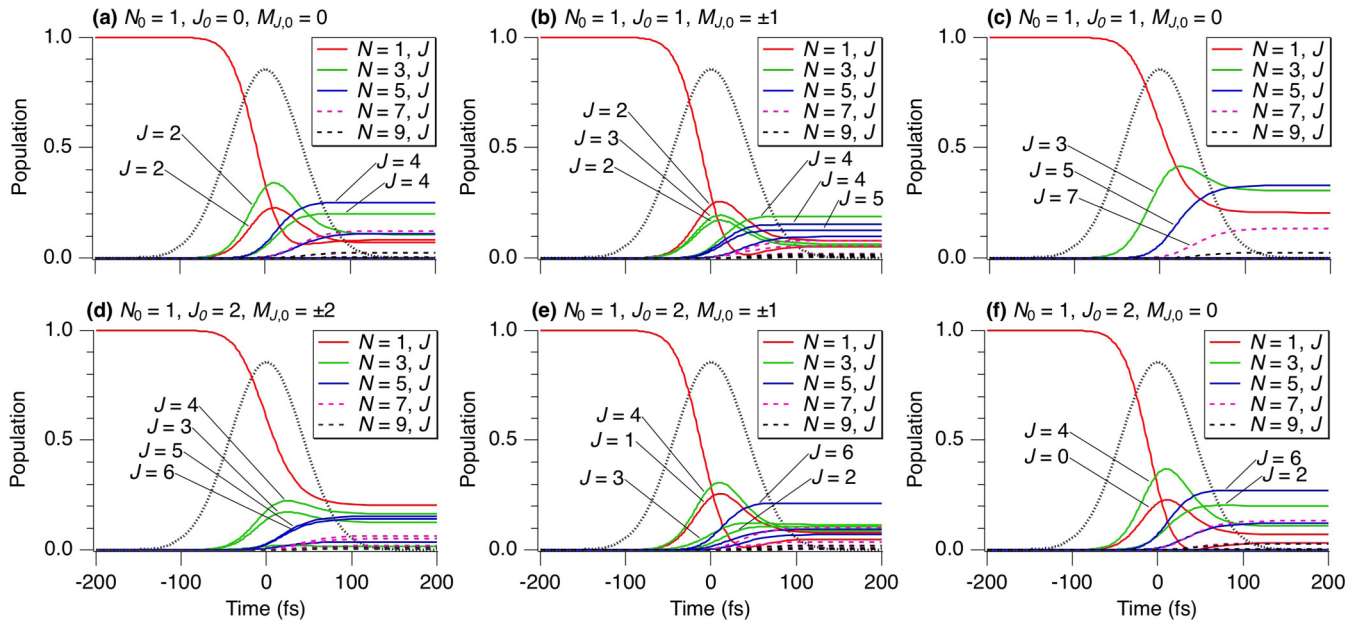


FIG. 5. The time evolution of the rotational population. The initial states are (a)  $N_0 = 1, J_0 = 0, M_{J,0} = 0$ , (b)  $N_0 = 1, J_0 = 1, M_{J,0} = \pm 1$ , (c)  $N_0 = 1, J_0 = 1, M_{J,0} = 0$ , (d)  $N_0 = 1, J_0 = 2, M_{J,0} = \pm 2$ , (e)  $N_0 = 1, J_0 = 2, M_{J,0} = \pm 1$ , and (f)  $N_0 = 1, J_0 = 2, M_{J,0} = 0$ . The dotted black curves show the intensity profile of the laser pulse with the peak intensity of  $30$  TW/cm<sup>2</sup> and the pulse width of  $100$  fs.

is used for the spin-dependent model, where  $\Lambda$ ,  $\Sigma$ , and  $\Omega = \Lambda + \Sigma$  are the projection of the electronic orbital, spin, and the total angular momenta onto a molecular axis, respectively;  $\langle \theta, \phi | J, \Omega, M_J \rangle = (-1)^{M_J - \Omega} \sqrt{\frac{2J+1}{4\pi}} D_{-M_J - \Omega}^J(\phi, \theta, 0)$  is the angular representation of a Hund's case (a) rotational wave function; and  $D_{M_J \Omega}^J(\phi, \theta, 0)$  is Wigner's rotational matrix [56].

The angular distributions,  $P(\theta)$ , for the two models are almost the same at  $t = 1.0$  ps as shown in Fig. 4(a). This is consistent because the rotational dynamics within 5 ps are similar to each other as mentioned above. However, at  $t = 8.1$  ps, where the difference of  $\langle \cos^2 \theta \rangle(t)$  between the spin-dependent and -independent models takes the maximum value of  $-0.07$  as shown in the upper panel of Fig. 3, the angular distributions of the molecular axis are remarkably different as shown in Fig. 4(b). The angular distributions in Fig. 4(c) are different around  $\theta = 0$  and  $\pi$  at  $t = 17.2$  ps although the difference of  $\langle \cos^2 \theta \rangle(t)$  is zero as shown in the upper panel of Fig. 3. It is found that the angular distribution, i.e., the rotational wave-packet motion, depends on the models. However, such difference does not affect calculations where molecular orientations have to be integrated over  $0 \leq \theta \leq \pi$  because differences around  $\theta = 0$  and  $\pi$  will be washed out by a Jacobian,  $\sin \theta$ . Our results show that the triplet character of the rotational energy structure of  $O_2$  should not be ignored for the rotational dynamics. Generally, in the multiplet electronic states, for example, the doublet states such as NO and  $N_2^+$  in the electronic ground  $X^2\Pi$  states, an electronic spin influences rotational dynamics.

Finally, rotational excitation processes based on the spin-dependent model are discussed. The time evolution of rotational populations,  $|c_{N_0, J_0, M_{J,0}}^{N_0, J_0, M_{J,0}}(t)|^2$ , for some initial rotational states,  $N_0$ ,  $J_0$ , and  $M_{J,0}$ , is shown in Fig. 5. When the initial state is  $N_0 = 1, J_0 = 0$ , and  $M_{J,0} = 0$ , as shown in Fig. 5(a), the state populations start to be transferred from the initial state to  $(N, J) = (1, 2)$  and  $(3, 2)$  simultaneously around  $-80$  fs. Since the selection rules for the interaction with the laser pulse are  $\Delta N = 0, \pm 2, \Delta J = 0, \pm 2$ , and  $\Delta M = 0$  in the case of  $M_{J,0} = 0$  as mentioned in Sec. II, the initial state  $(1, 0)$  couples with not  $(1, 1)$ ,  $(3, 3)$ , and  $(3, 4)$  states but only  $(1, 2)$  and  $(3, 2)$  states. Then, these populations of  $(1, 2)$  and  $(3, 2)$  start to be transferred to  $(3, 4)$  and  $(5, 4)$  around  $-30$  fs. After that, populations of  $(3, 4)$  and  $(5, 4)$  are transferred to  $(5, 6)$  and  $(7, 6)$  around 0 fs.

In order to study the excitation process in detail, a part of the matrix element in Eq. (13),

$$S = \sqrt{(2J_1 + 1)(2J_2 + 1)(2N_1 + 1)(2N_2 + 1)} \\ \times \begin{pmatrix} J_1 & 2 & J_2 \\ -M_{J_1} & 0 & M_{J_2} \end{pmatrix} \begin{pmatrix} N_1 & 2 & N_2 \\ 0 & 0 & 0 \end{pmatrix} \begin{Bmatrix} N_1 & J_1 & 1 \\ J_2 & N_2 & 2 \end{Bmatrix}, \quad (23)$$

which is proportional to the interaction matrix element,  $\langle (N_1 S) J_1 M_{J_1} | \hat{V}(t) | (N_2 S) J_2 M_{J_2} \rangle$ , is calculated. Figure 6 shows the values of  $|S|$  between arrowed states for (a)  $M_J = 0$ , (b)  $M_J = \pm 1$ , and (c)  $M_J = \pm 2$ . For the sake of simplicity,  $S$  values more than 0.2 are depicted. In Fig. 6, the energy levels are described separately by  $F_1$ ,  $F_2$ , and  $F_3$  states, which

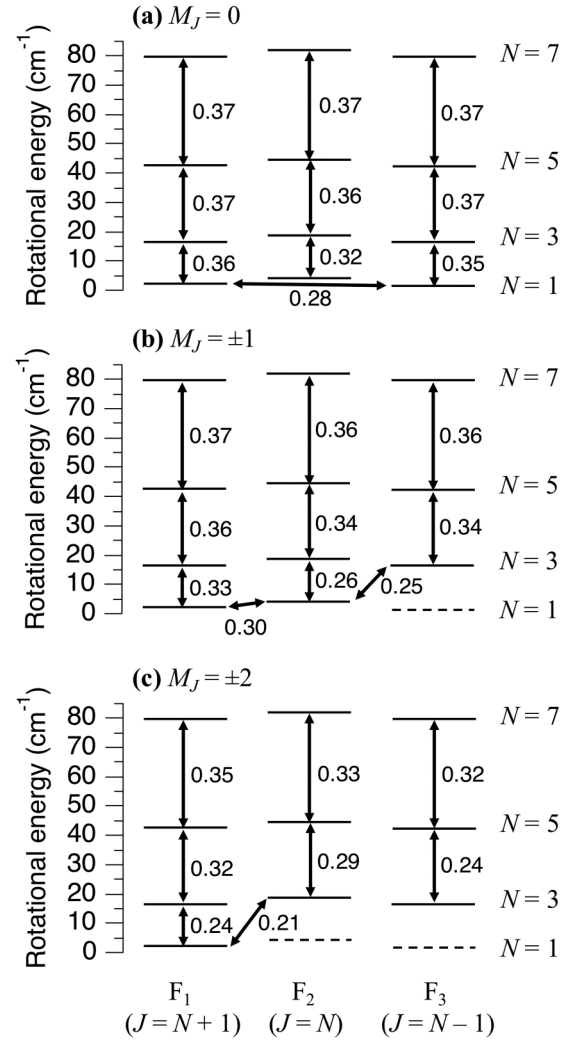


FIG. 6. The matrix elements between arrowed states for (a)  $M_J = 0$ , (b)  $M_J = \pm 1$ , and (c)  $M_J = \pm 2$ . The initial  $M_{J,0}$  is conserved due to the axial symmetry of the linear laser polarization.

corresponds to  $J = N + 1$ ,  $J = N$ , and  $J = N - 1$  states, respectively [57].

As mentioned before, the population of the initial state  $(1, 0)$  with  $M_{J,0} = 0$  is initially transferred to  $(1, 2)$  and  $(3, 2)$  as shown in Fig. 5(a). Since the interaction between  $(1, 0)$  and  $(3, 2)$ ,  $|S| = 0.35$ , is larger than that between  $(1, 0)$  and  $(1, 2)$ ,  $|S| = 0.28$ , as shown in Fig. 6(a), population transfer from  $(1, 0)$  to  $(3, 2)$  takes place more effectively than that from  $(1, 0)$  to  $(1, 2)$ . Then,  $(3, 2)$  couples strongly with  $(5, 4)$  due to the large value of  $|S| = 0.37$ . On the other hand,  $(1, 2)$  interacts with  $(3, 4)$  according to  $|S| = 0.36$ . In the next excitation, populations for the generated  $(5, 4)$  and  $(3, 4)$  states are transferred to  $(7, 6)$  and  $(5, 6)$ , respectively. As a result, the initial-state population is transferred through two different pathways,  $(1, 0) \rightarrow (3, 2) \rightarrow (5, 4) \rightarrow (7, 6) \rightarrow \dots$  and  $(1, 0) \rightarrow (1, 2) \rightarrow (3, 4) \rightarrow (5, 6) \rightarrow \dots$ . It should be noted that such bifurcated pathways have been reported for the rotational excitation of NO in the electronic ground  $X^2\Pi$  state [54,55] and benzene in the electronic ground  $^1S_0$  state [58] induced by an intense nonresonant femtosecond laser pulse.

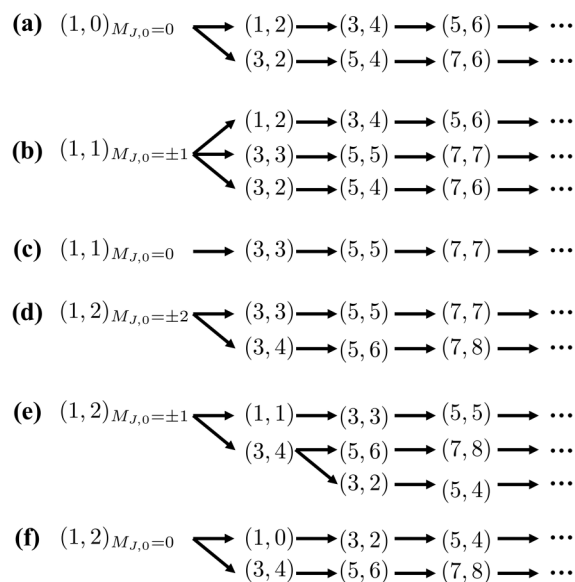


FIG. 7. The excitation processes starting from nine initial states induced by the intense laser field. The values in parentheses represent the quantum numbers of the rotational and total angular momentum,  $N, J$ , respectively, as  $(N, J)$ . The subscript  $M_{J,0}$  stands for the initial  $M_J$ , which is conserved.

Similarly, the excitation processes for the initial states in Figs. 5(a)–5(f) are revealed as shown in Figs. 7(a)–7(f), respectively. When the initial state is  $(1, 1)_{M_{J,0}=\pm 1}$ , the excitation pathway splits into three, as shown in Fig. 7(b), because the initial state initially interacts with three states,  $(1, 2)$ ,  $(3, 3)$ , and  $(3, 2)$ . When the initial state is  $(1, 1)_{M_{J,0}=0}$ , the excitation pathway does not bifurcate because the initial state couples with only  $(3, 3)$  due to the selection rules,  $\Delta N = 0, \pm 2$ ,

$\Delta J = 0, \pm 2$ . Consequently, the excitation process is simplified. Such simple excitation has been reported for N<sub>2</sub> in the electronic ground  $X^1\Sigma_g^+$  state [51]. On the other hand, when the initial state is  $(1, 2)_{M_{J,0}=\pm 1}$ , the excitation process is complicated by two bifurcations.

#### IV. CONCLUSION

We investigated rotational dynamics of O<sub>2</sub> in the electronic  $X^3\Sigma_g^-$  state induced by an intense femtosecond laser field. The rotational dynamics calculated by two different models including the triplet character of O<sub>2</sub> (spin-dependent model) or not (spin-independent model) were compared. We found that the final rotational population after the interaction does not depend on the models. On the other hand, we found that the rotational dynamics evaluated by alignment degrees and angular distributions of molecular axes depend on the models. Although the rotational dynamics calculated by the spin-independent model is similar to that calculated by the spin-dependent model within 5 ps, the triplet splittings in the rotational energy levels affect the rotational dynamics after 5 ps. This is explained by the inverse of the energy difference between triplet splittings in the rotational levels. We showed that the multiplet energy splittings in rotational energies should be included when the rotational dynamics in the multiplet electronic state are considered. We also investigated the excitation processes and found the excitation pathways with single and double bifurcation depending on the initial state.

#### ACKNOWLEDGMENT

This work was supported by Japan Society for the Promotion of Science KAKENHI Grant No. 17K05593.

- [1] H. Stapelfeldt and T. Seideman, Colloquium: Aligning molecules with strong laser pulses, *Rev. Mod. Phys.* **75**, 543 (2003).
- [2] T. Seideman and E. Hamilton, Nonadiabatic alignment by intense pulses: Concepts, theory, and directions, *Adv. Atom. Mol. Opt. Phys.* **52**, 289 (2005).
- [3] Y. Ohshima and H. Hasegawa, Coherent rotational excitation by intense nonresonant laser fields, *Int. Rev. Phys. Chem.* **29**, 619 (2010).
- [4] C. H. Lin, J. P. Heritage, and T. K. Gustafson, Susceptibility echos in linear molecular gases, *Appl. Phys. Lett.* **19**, 397 (1971).
- [5] I. Sh. Averbukh and R. Arvieu, Angular Focusing, Squeezing, and Rainbow Formation in a Strongly Driven Quantum Rotor, *Phys. Rev. Lett.* **87**, 163601 (2001).
- [6] T. Seideman, Rotational excitation and molecular alignment in intense laser fields, *J. Chem. Phys.* **103**, 7887 (1995).
- [7] J. P. Heritage, T. K. Gustafson, and C. H. Lin, Observation of Coherent Transient Birefringence in CS<sub>2</sub> Vapor, *Phys. Rev. Lett.* **34**, 1299 (1975).
- [8] F. Rosca-Pruna and M. J. J. Vrakking, Experimental Observation of Revival Structures in Picosecond Laser-Induced Alignment of I<sub>2</sub>, *Phys. Rev. Lett.* **87**, 153902 (2001).
- [9] T. Kanai, S. Minemoto, and H. Sakai, Quantum interference during high-order harmonic generation from aligned molecules, *Nature (London)* **435**, 470 (2005).
- [10] V. Renard, M. Renard, S. Gu erin, Y. T. Pashayan, B. Lavorel, O. Faucher, and H. R. Jauslin, Postpulse Molecular Alignment Measured by a Weak Field Polarization Technique, *Phys. Rev. Lett.* **90**, 153601 (2003).
- [11] P. Peng, Y. Bai, N. Li, and P. Liu, Measurement of field-free molecular alignment by balanced weak field polarization technique, *AIP Adv.* **5**, 127205 (2015).
- [12] K. Mizuse, N. Chizuwa, D. Ikeda, T. Imajo, and Y. Ohshima, Visualizing rotational wave functions of electronically excited nitric oxide molecules by using an ion imaging technique, *Phys. Chem. Chem. Phys.* **20**, 3303 (2018).
- [13] E. T. Karamatskos, S. Raabe, T. Mullins, A. Trabattoni, P. Stammer, G. Goldsztejn, R. R. Johansen, K. Długoł cki, H. Stapelfeldt, Marc J. J. Vrakking, S. Trippel, A. Rouz e, and J. K upper, Molecular movie of ultrafast coherent rotational dynamics of OCS, *Nat. Commun.* **10**, 3364 (2019).
- [14] P. W. Dooley, I. V. Litvinyuk, K. F. Lee, D. M. Rayner, M. Spanner, D. M. Villeneuve, and P. B. Corkum, Direct imaging of rotational wave-packet dynamics of diatomic molecules, *Phys. Rev. A* **68**, 023406 (2003).

- [15] K. Miyazaki, M. Kaku, G. Miyaji, A. Abdurrouf, and F. H. M. Faisal, Field-Free Alignment of Molecules Observed with High-Order Harmonic Generation, *Phys. Rev. Lett.* **95**, 243903 (2005).
- [16] V. G. Stavros, E. Harel, and S. R. Leone, The influence of intense control laser pulses on homodyne-detected rotational wave packet dynamics in O<sub>2</sub> by degenerate four-wave mixing, *J. Chem. Phys.* **122**, 064301 (2005).
- [17] D. Pinkham and R. R. Jones, Intense laser ionization of transiently aligned co, *Phys. Rev. A* **72**, 023418 (2005).
- [18] W. A. Bryan, E. M. L. English, J. McKenna, J. Wood, C. R. Calvert, I. C. E. Turcu, R. Torres, J. L. Collier, I. D. Williams, and W. R. Newell, Mapping the evolution of optically generated rotational wave packets in a room-temperature ensemble of D<sub>2</sub>, *Phys. Rev. A* **76**, 023414 (2007).
- [19] A. Goban, S. Minemoto, and H. Sakai, Laser-Field-Free Molecular Orientation, *Phys. Rev. Lett.* **101**, 013001 (2008).
- [20] I. A. Bocharova, H. Mashiko, M. Magrakoveldze, D. Ray, P. Ranitovic, C. L. Cocke, and I. V. Litvinyuk, Direct coulomb-explosion imaging of coherent nuclear dynamics induced by few-cycle laser pulses in light and heavy hydrogen, *Phys. Rev. A* **77**, 053407 (2008).
- [21] D. W. Broege, R. N. Coffee, and P. H. Bucksbaum, Strong-field impulsive alignment in the presence of high temperatures and large centrifugal distortion, *Phys. Rev. A* **78**, 035401 (2008).
- [22] M. Comstock, V. Senekerimyan, and M. Dantus, Ultrafast laser induced molecular alignment and deformation: Experimental evidence from neutral molecules and from fragment ions, *J. Phys. Chem. A* **107**, 8271 (2003).
- [23] A. Rouzée, V. Renard, S. Guérin, O. Faucher, and B. Lavorel, Optical gratings induced by field-free alignment of molecules, *Phys. Rev. A* **75**, 013419 (2007).
- [24] Y. Gao, C. Wu, N. Xu, G. Zeng, H. Jiang, H. Yang, and Q. Gong, Manipulating molecular rotational wave packets with strong femtosecond laser pulses, *Phys. Rev. A* **77**, 043404 (2008).
- [25] C. Z. Bisgaard, O. J. Clarkin, G. Wu, Anthony M. D. Lee, O. Geßner, C. C. Hayden, and A. Stolow, Time-resolved molecular frame dynamics of fixed-in-space CS<sub>2</sub> molecules, *Science* **323**, 1464 (2009).
- [26] P. Peng, N. Li, J. Li, H. Yang, P. Liu, R. Li, and Z. Xu, Spectral modulation of high-order harmonic generation from prealigned CO<sub>2</sub> molecules, *Opt. Lett.* **38**, 4872 (2013).
- [27] E. Hamilton, T. Seidema, T. Ejdrup, M. D. Poulsen, C. Z. Bisgaard, S. S. Viftrup, and H. Stapelfeldt, Alignment of symmetric top molecules by short laser pulses, *Phys. Rev. A* **72**, 043402 (2005).
- [28] C. Z. Bisgaard, S. S. Viftrup, and H. Stapelfeldt, Alignment enhancement of a symmetric top molecule by two short laser pulses, *Phys. Rev. A* **73**, 053410 (2006).
- [29] H. Hasegawa and Y. Ohshima, Quantum State Reconstruction of a Rotational Wave Packet Created by a Nonresonant Intense Femtosecond Laser Field, *Phys. Rev. Lett.* **101**, 053002 (2008).
- [30] D. Baek, H. Hasegawa, and Y. Ohshima, Unveiling the nonadiabatic rotational excitation process in a symmetric-top molecule induced by two intense laser pulses, *J. Chem. Phys.* **134**, 224302 (2011).
- [31] E. Péronne, M. D. Poulsen, C. Z. Bisgaard, H. Stapelfeldt, and T. Seideman, Nonadiabatic Alignment of Asymmetric Top Molecules: Field-Free Alignment of Iodobenzene, *Phys. Rev. Lett.* **91**, 043003 (2003).
- [32] C. Z. Bisgaard, M. D. Poulsen, E. Péronne, S. S. Viftrup, and H. Stapelfeldt, Observation of Enhanced Field-Free Molecular Alignment by Two Laser Pulses, *Phys. Rev. Lett.* **92**, 173004 (2004).
- [33] M. D. Poulsen, E. Péronne, H. Stapelfeldt, C. Z. Bisgaard, S. S. Viftrup, E. Hamilton, and T. Seideman, Nonadiabatic alignment of asymmetric top molecules: Rotational revivals, *J. Chem. Phys.* **121**, 783 (2004).
- [34] E. Péronne, M. D. Poulsen, H. Stapelfeldt, C. Z. Bisgaard, E. Hamilton, and T. Seideman, Nonadiabatic laser-induced alignment of iodobenzene molecules, *Phys. Rev. A* **70**, 063410 (2004).
- [35] A. Rouzée, S. Guérin, V. Boudon, B. Lavorel, and O. Faucher, Field-free one-dimensional alignment of ethylene molecule, *Phys. Rev. A* **73**, 033418 (2006).
- [36] L. Holmegaard, S. S. Viftrup, V. Kumarappan, C. Z. Bisgaard, H. Stapelfeldt, E. Hamilton, and T. Seideman, Control of rotational wave-packet dynamics in asymmetric top molecules, *Phys. Rev. A* **75**, 051403(R) (2007).
- [37] D. Pavičić, K. F. Lee, D. M. Rayner, P. B. Corkum, and D. M. Villeneuve, Direct Measurement of the Angular Dependence of Ionization for N<sub>2</sub>, O<sub>2</sub>, and CO<sub>2</sub> in Intense Laser Fields, *Phys. Rev. Lett.* **98**, 243001 (2007).
- [38] X. Xie, K. Doblhoff-Dier, H. Xu, S. Roither, M. S. Schöffler, H. Kartashov, S. Erattupuzha, T. Rathje, G. G. Paulus, K. Yamanouchi, A. Baltuška, S. Gráfe, and M. Kitzler, Selective Control Over Fragmentation Reactions in Polyatomic Molecules Using Impulsive Laser Alignment, *Phys. Rev. Lett.* **112**, 163003 (2014).
- [39] H. Hasegawa, Y. Ikeda, K. Sonoda, T. Sato, A. Iwasaki, and K. Yamanouchi, Angular dependence of ionization probability of C<sub>2</sub>H<sub>2</sub> in a linearly polarized intense laser field, *Chem. Phys. Lett.* **662**, 235 (2016).
- [40] O. Ghafur, A. Rouzée, A. Gijsbertsen, W. K. Siu, S. Stolte, and M. J. J. Vrakking, Impulsive orientation and alignment of quantum-state-selected no molecules, *Nat. Phys.* **5**, 289 (2009).
- [41] D. Sofikitis, L. Rubio-Lago, M. R. Martin, D. J. Ankeny Brown, N. C.-M. Bartlett, A. J. Alexander, R. N. Zare, and T. P. Rakitzis, Optical control of ground-state atomic orbital alignment: Cl(<sup>2</sup>P<sub>3/2</sub>) atoms from hcl (*v* = 2, *j* = 1) photodissociation, *J. Chem. Phys.* **127**, 144307 (2007).
- [42] E. F. Thomas, A. A. Søndergaard, B. Shepperson, N. E. Henriksen, and H. Stapelfeldt, Hyperfine-Structure-Induced Depolarization of Impulsively Aligned I<sub>2</sub> Molecules, *Phys. Rev. Lett.* **120**, 163202 (2018).
- [43] J. Itatani, D. Zeidler, J. Levesque, M. Spanner, D. M. Villeneuve, and P. B. Corkum, Controlling High Harmonic Generation with Molecular Wave Packets, *Phys. Rev. Lett.* **94**, 123902 (2005).
- [44] A. Korobenko, A. A. Milner, and V. Milner, Direct Observation, Study, and Control of Molecular Superrotors, *Phys. Rev. Lett.* **112**, 113004 (2014).
- [45] J. Floß and I. Sh. Averbukh, Molecular spinning by a chiral train of short laser pulses, *Phys. Rev. A* **86**, 063414 (2012).
- [46] A. A. Milner, A. Korobenko, and V. Milner, Coherent spin-rotational dynamics of oxygen superrotors, *New J. Phys.* **16**, 093038 (2014).
- [47] T. L. Courtney and C. J. Kliewer, Rotational coherence beating in molecular oxygen: Coupling between electronic spin and nuclear angular momenta, *J. Chem. Phys.* **149**, 234201 (2018).



- [48] J. Brown and A. Carrington, *Rotational Spectroscopy of Diatomic Molecules* (Cambridge University, Cambridge, England, 2003).
- [49] H. Lefebvre-Brion and R. W. Field, *The Spectra and Dynamics of Diatomic Molecules* (Elsevier, Amsterdam, 2004).
- [50] R. Schlapp, Fine structure in the  $^3\Sigma$  ground state of the oxygen molecule, and the rotational intensity distribution in the atmospheric oxygen band, *Phys. Rev.* **51**, 342 (1937).
- [51] M. Tsubouchi and T. Suzuki, Photoionization of homonuclear diatomic molecules aligned by an intense femtosecond laser pulse, *Phys. Rev. A* **72**, 022512 (2005).
- [52] W. M. Welch and M. Mizushima, Molecular parameters of the O<sub>2</sub> molecule, *Phys. Rev. A* **5**, 2692 (1972).
- [53] J. W. C. Johns and D. W. Leppard, Calculation of rotation-electronic energies and relative transition intensities in diatomic molecules, *J. Mol. Spectrosc.* **55**, 374 (1975).
- [54] H. Hasegawa and Y. Ohshima, Decoding the state distribution in a nonadiabatic rotational excitation by a nonresonant intense laser field, *Phys. Rev. A* **74**, 061401(R) (2006).
- [55] A. S. Meijer, Y. Zhang, D. H. Parker, W. J. van der Zande, A. Gijsbertsen, and M. J. J. Vrakking, Controlling rotational state distributions using two-pulse stimulated raman excitation, *Phys. Rev. A* **76**, 023411 (2007).
- [56] R. N. Zare, *Angular Momentum* (Wiley, New York, 1988).
- [57] G. Herzberg, *Molecular Spectra and Molecular Structure: Volume I Spectra of Diatomic Molecules* (Krieger, 1950).
- [58] H. Hasegawa and Y. Ohshima, Nonadiabatic rotational excitation of benzene by nonresonant intense femtosecond laser fields, *Chem. Phys. Lett.* **454**, 148 (2008).